

Relocation of the foreshocks and aftershocks of the 2021

*Ms*6.4 Yangbi earthquake sequence, Yunnan, China

Ting Yang¹, Boren Li¹, Lihua Fang^{1,2,3*}, Youjin Su⁴, Yusheng Zhong⁴, Jingqiong Yang⁴, Min Qin⁴, Yaji Xu⁴

1. *Institute of Geophysics, China Earthquake Administration, Beijing 100081, China*

2. *Key Laboratory of Earthquake source physics, China Earthquake Administration, Beijing 100081, China*

3. *Institute of disaster prevention, Sanhe 065201, China*

4. *Yunnan Earthquake Agency, Kunming 650224, China*

ABSTRACT: An *Ms*6.4 earthquake occurred in Yangbi, Yunnan, China on May 21, 2021, which has obvious foreshock activity and abundant aftershocks. Based on the seismic observation data recorded by the Yunnan seismic network three days before and seven days after the mainshock, a double-difference location method was used to relocate 2133 earthquakes of the Yangbi sequence. Aftershocks are mostly distributed to the southeast of the mainshock in a unilateral rupture pattern. This sequence exhibits a SE-trending linear alignment with a length of about 25 km, and most of the focal depth is above 12 km. Integrated with the seismic distribution and focal mechanism results, we infer that the strike of the seismogenic fault is about 140°, and dipping to the SW. The fault structure revealed by the seismic sequence is complex, with the NW segment exhibiting a steep dip and relatively simple structure of strike-slip rupture and the SE segment consisting of several branching ruptures. The Yangbi earthquake is a typical foreshock-mainshock-aftershock sequence, and the mainshock is likely triggered by the largest foreshock. This earthquake occurred in the boundary between high- and low-velocity anomalous zones, where is susceptible to generate large earthquakes.

KEY WORDS: Yangbi earthquake, Weixi-Qiaohou-Weishan fault, earthquake sequence, double-difference relocation.

0 INTRODUCTION

According to the China Earthquake Networks Center, an earthquake of magnitude $M_s6.4$ occurred in Yangbi County, Dali City, Yunnan Province at 21:48 on May 21, 2021 (Beijing time). The epicenter location is 25.67°N , 99.87°E , and the focal depth is 8 km. A series of small and medium-sized foreshocks occurred near the epicenter three days before the mainshock, including five foreshocks with $M \geq 4$, and the largest foreshock of $M_s5.6$ occurred about 27 minutes before the mainshock. A total of 3164 aftershocks were recorded by the Yunnan Seismic Network by the end of 08:00 on May 28. Among them, there are two aftershocks with $M \geq 5$, with the largest one of $M_s5.2$. This earthquake shows a typical foreshock-mainshock-aftershock sequence. The maximum intensity of the earthquake is VIII, and the total area with the intensity \geq VI is about 6600 km^2 . The long axis of isoseismic line is in the NNW and about 106 km, and the short axis is about 76 km (http://www.yndzj.gov.cn/yndzj/_300559/300651/629959/index.html). Three people was killed and 32 injured in this earthquake, and the economic loss exceeded 3.1 billion yuan (<https://baijiahao.baidu.com/s?id=1700414612337125458&wfr=spider&for=pc>).

The Yangbi earthquake occurred near the Weixi-Qiaohou-Weishan fault, which starts from Weixi County in the north and ends at Weishan County in the south, with a total length of about 280 km. The strike of the fault is in the NW direction, dipping to the SW or NE, with dip angles of 60° - 80° (Tang and Chang, 2013). As the eastern boundary fault of the Lanping-Simao depression, Mesozoic sedimentary layers were extensively developed on its western side and Paleozoic and Cangshan metamorphic zone in the east (Institute of Geology, National Seismological Bureau, et al., 1990). The Weixi-Qiaohou-Weishan fault is connected to the Jinsha River fault to the north and the Red River fault to the south, which together form the western boundary zone of the Sichuan-Yunnan rhombic block (Chang et al., 2016b). Seismicity of this boundary zone is frequent, and an $M7.0$ Dali earthquake occurred on March 16, 1925. The Weixi-Qiaohou-Weishan fault can be divided into three segments. During the neotectonic period, the middle and northern segment was dominated by the dextral strike-slip fault, while the southern segment was dominated by the normal fault (Chang et al., 2016a). The Yangbi earthquake occurred in the middle segment of the Weixi-Qiaohou-Weishan fault (Fig. 1), which has exhibited dextral strike-slip and normal faulting activity, with an average horizontal slip rate of 1.25 mm/a since the Quaternary (Ren et al.,

2007).

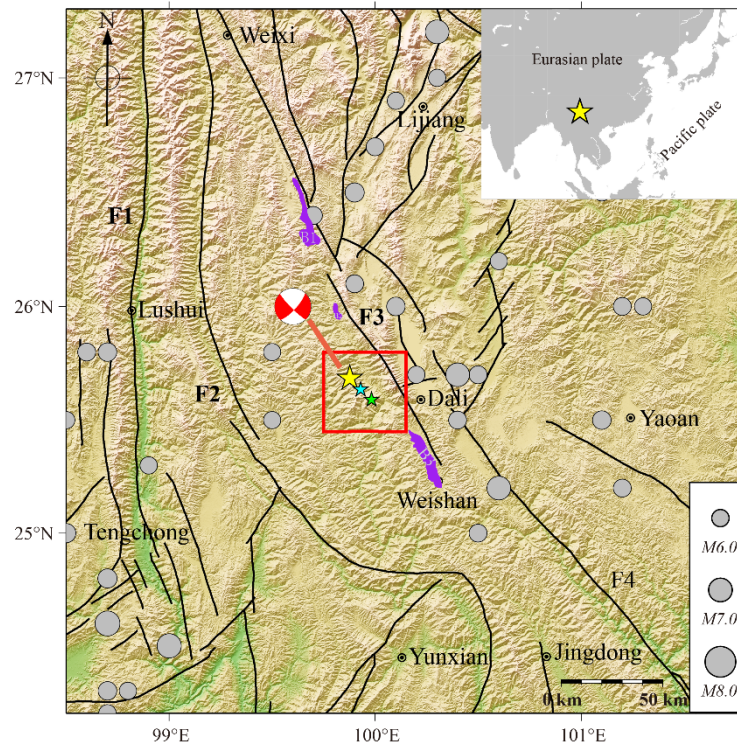


Figure 1. Distribution of the epicenters of the Yangbi earthquake and faults in the study area.

Faults (black lines) — F1: Nujiang fault, F2: Lancangjiang fault, F3: Weixi-Qiaohou-Weishan fault, F4: Red River fault. Quaternary Basins along the F3 (purple zones) — B1: Madeng basin, B2: Liantie basin, B3: Weishan basin.

The yellow circles indicate historical earthquakes of $M \geq 6.0$ since 26 BC (The Earthquake Disaster Prevention Department of China Earthquake Administration, 1999a; 1999b). The red rectangle represents the earthquake relocation study area. The big yellow star, small cyan and magenta stars indicate the mainshock, the largest foreshock and the largest aftershock, respectively. The focal mechanism of the mainshock is determined by USGS.

The inset indicates the location of the mainshock.

After the earthquake, the China Earthquake Administration quickly organized earthquake scientific investigation, portable seismic observations and earthquake potential consultations, and domestic and foreign scholars also immediately carried out research on the seismogenic structure, sequence characteristics and source mechanisms of this earthquake sequence using various methods such as seismic, geological and geodetic measurements. This study focuses on the research of relocation of the foreshock-mainshock-aftershock sequence of the Yangbi earthquake. The results can provide valuable information for studying the seismogenic structure of the Yangbi earthquake, analyzing the spatial and temporal distribution characteristics of aftershock activities, and determining the trend of aftershock activities.

1 SEISMIC STATIONS AND DATA

101 seismic stations from regional permanent and temporary stations were used in this study. There are 10 seismic stations within 100 km near the epicenter of the mainshock (Fig. 2a). The Yangbi earthquake sequence is well-covered by nearby seismic stations and ensured the reliability of the seismic location results. Real-time waveform data were transmitted to the Yunnan Seismic Network and processed uniformly. The seismic phase-picking data and initial hypocenter locations used in this study are from the observation bulletin of the Yunnan Seismic Network.

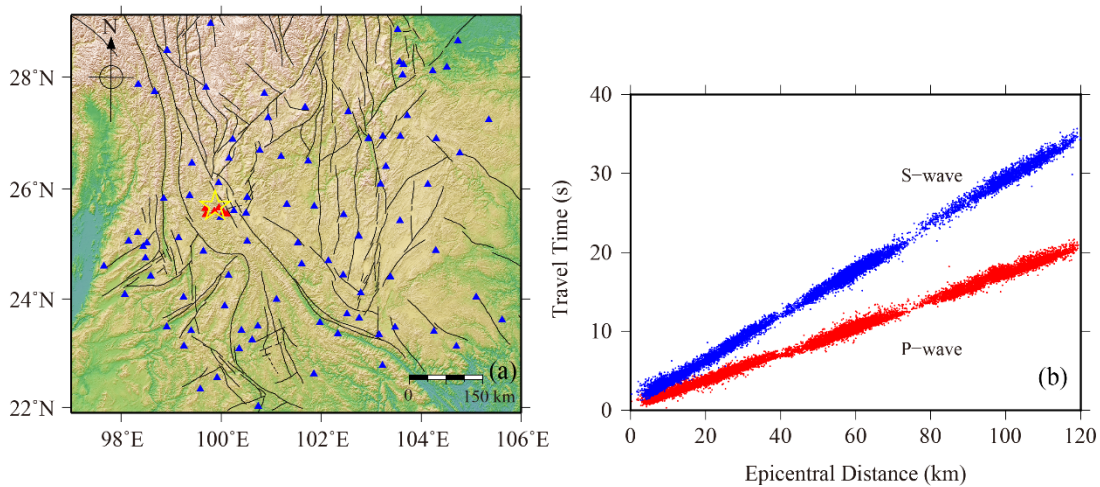


Figure 2. (a) Distribution of seismic stations. The blue and red triangles show the location of the permanent and temporary seismic stations. The hollow yellow star denotes the mainshock. The black lines are present the faults. (b) Travel time curves of P- and S-wave. The dots represent epicentral distance versus travel time for source-receiver pairs. The red and blue curves indicate P- and S-wave, respectively.

3,545 earthquakes with magnitude range of M -1.8 to 6.4 were recorded by the Yunnan Seismic Network from May 18, 2021 to May 28, 2021. In order to obtain precise location results, we selected earthquakes with phase number ≥ 10 and maximum gap angle $\leq 180^\circ$ for relocation. There are 2,153 earthquakes that met this criterion. The statistical analysis of the observation bulletin shows that the error of the P- and S-wave arrival times and the initial location error are small, indicating high quality of the observation bulletin. Figure 2b shows the travel time curves of P-wave and S-wave. The initial earthquake location results from Yunnan seismic network is dispersed in the study area (Fig. 3). The aftershocks show concentration in some depths (Fig. 3), which is usually found in absolute location with a 1-D velocity model.

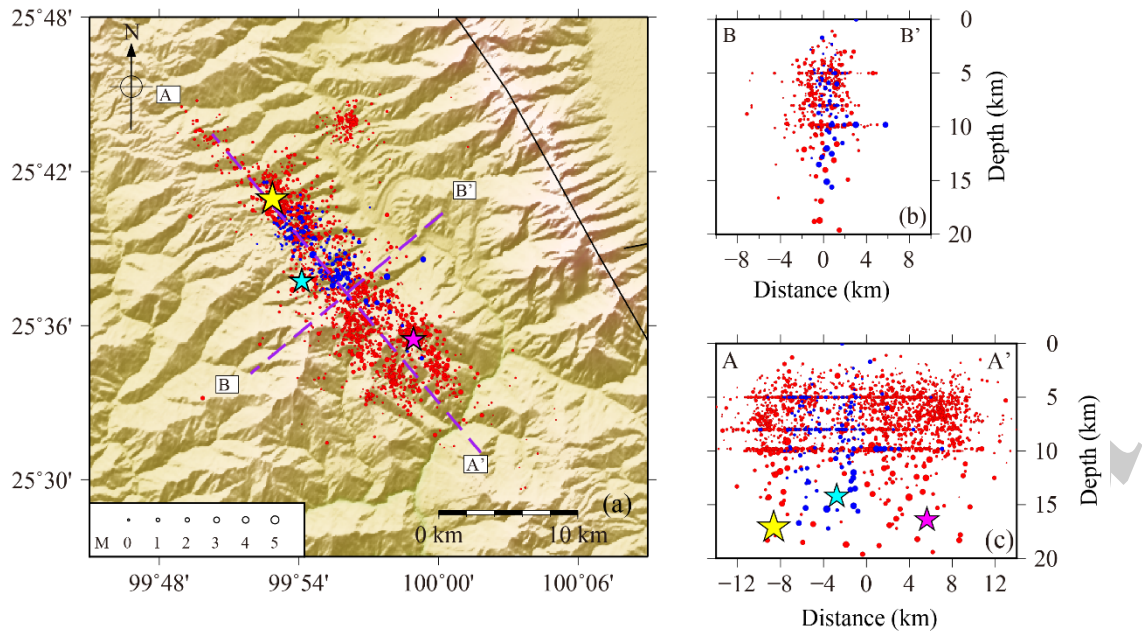


Figure 3. Distribution of initial location of foreshocks and aftershocks in plane view and cross-section profiles along AA' and BB'. The big yellow star denotes the mainshock, and the cyan and magenta stars represent the largest foreshock and the largest aftershock, respectively. Blue and red dots represent foreshocks and aftershocks. The distance from each earthquake to the profile BB' is less than 2.5 km. Earthquakes scale with the magnitudes.

2 RELOCATION OF THE EARTHQUAKE SEQUENCE

Relative location method is an effective way to locate events relative to a well determined event, applied in both natural earthquake and nuclear event location (Fang et al., 2015; Wang and Hutko, 2018). We used the double-difference location method (Waldhauser and Ellsworth, 2000), one of the relative location methods to relocate the earthquake sequence of the Yangbi earthquake. Firstly, the earthquake pairs were composed according to the initial source location. Then a group of adjacent phases that are close to each other at the same station were selected, and their traveltimes differences were used to invert the source location, thus can better eliminate the common propagation path effect between the source and the station. In addition, this method is less dependent on the velocity model. This method has been widely used in the relocation of earthquake sequences and earthquake swarms in China and abroad (Chen et al., 2009; Yu et al., 2010; Zhao et al., 2013; Zhang et al., 2014; Fang et al., 2018; Momeni and Tatar, 2018; Xie et al., 2018; Lanza et al., 2019; Li et al., 2019; Yi et al., 2019).

Velocity model is a key element in earthquake location. If the velocity model is not appropriate for the study area, the amount of the final relocated earthquakes will be small and the

error will be large, thus the result may be unreliable. Several velocity models are available near the Yangbi area, including the models of Bai and Wang (2004), Laske et al. (2013), Chen et al. (2016), and Liu et al., (2021). Among them, the seismic sounding profile from Zhefang to Binchuan crosses the study area (Bai and Wang, 2004), and the other seismic sounding profile from Yunxian to Ninglang is slightly distant away from the study region (Chen et al., 2016). The 3D community velocity model (SWChinaCVM) of Sichuan-Yunnan region was recently established by using the joint inversion of body-wave travel time data and Rayleigh surface wave dispersion data (Liu et al. 2021).

We used different velocity models to relocate these earthquakes and selected the optimal velocity model by comprehensively comparing the location results. The analysis of the relocation results shows that the velocity model of Bai and Wang (2004) is the best one for this study area, since the proportion of earthquake number after relocation is the highest and the location error and the residual error are the least in these four models (Bai and Wang, 2004; Laske et al., 2013; Chen et al., 2016; Liu et al., 2021). The final 1-D velocity model is shown in Table 1. The V_p/V_s ratio of 1.75 is derived with the $h-k$ stacking method of receiver function (Zhang and Gao, 2019; Zhang et al., 2020).

Table 1 1-D velocity model used in earthquake relocation

Top of the layer (km)	0	8	15	28	35	45
P-wave velocity ($\text{km}\cdot\text{s}^{-1}$)	5.6	6.1	6.45	6.55	7.15	7.8

There are 44,361 seismic phase data in the observation bulletin, including 25,271 P-wave and 19,090 S-wave phases, with an average of 20 seismic phase data per earthquake. The average values of the horizontal error, vertical error and residual of the initial location are 0.49 km, 1.49 km and 0.22 s, respectively, and the focal depth range is 0~21 km. In the process of composing the earthquake pairs, the minimum number of connections (MINLNK) and observations (MINOBS) are both set to 8, the source spacing is less than 10 km, and the distance between the earthquake pair and the station is less than 200 km. The weight of the P-wave and S-wave arrivals is 1.0 and 0.7, respectively.

3. RESULTS

Figure 4 shows the relocation results of 2,133 earthquakes by using the double-difference location method. The average location errors of the EW, NS, and vertical directions are 0.19 km, 0.20 km, and 0.27 km, respectively. The average RMS residual is 0.11 s. Compared with the initial location results from the Yunnan Seismic Network, the location error and residual are significantly reduced after relocation, and the distribution of the earthquakes is more concentrated and clustered (Figs. 3 and 4).

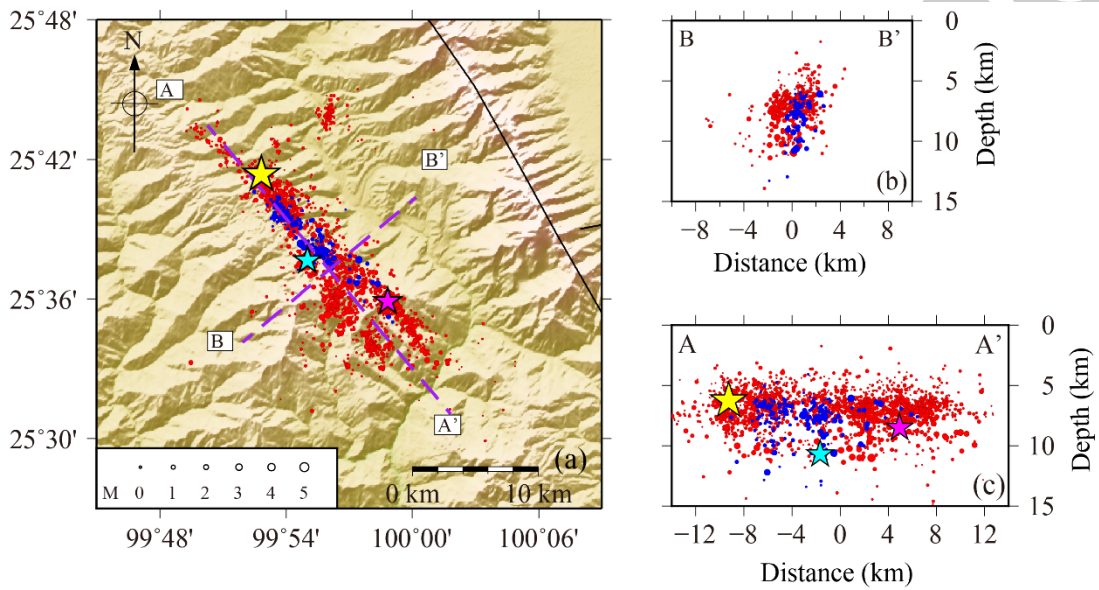


Figure 4. Distribution of relocated foreshocks and aftershocks in plane view and cross-section profiles along AA' and BB'. The big yellow star denotes the mainshock, and the cyan and magenta stars represent the largest foreshock and the largest aftershock, respectively. Blue and red dots represent foreshocks and aftershocks. The distance from each earthquake to the profile BB' is less than 2.5 km. Earthquakes scale with the magnitudes.

From the plane view (Fig. 4a), the earthquakes are linearly alignment in the northwest direction on the southwest side of the Weixi-Qiaohou-Weishan fault zone. The mainshock is located at the northwest end of the seismic sequence, showing a unilateral rupture pattern. The early aftershocks are linearly distributed in the NW-SE direction with a narrow width range, while the later aftershocks expanded to the SE direction with time and the aftershock zone becomes wider. The rupture length of the source area is about 25 km. The largest foreshock of $M_s5.6$ was located about 7 km to the SE direction of the mainshock, and the largest aftershock of $M_s5.2$ was located at the southeast end of the sequence. In addition, an earthquake of $M_s4.1$ occurred in the

northwestern region on May 27, 2021, which is about 5 km north of the main rupture zone. Afterwards, there is a small cluster of earthquakes around this earthquake.

The focal depths after relocation show that most earthquakes are distributed at depths shallower than 12 km. The focal depth of the mainshock is 5.6 km, and both the largest foreshock and the largest aftershock are located at the bottom of the seismic sequence. The distribution of the relocated earthquakes is more concentrated at depths of 5-8 km after using the data from newly deployed temporary seismic stations (red circles in Fig. 4c). A study on the Lushan earthquake sequence by Fang et al. (2015) also found that the aftershock distribution became more concentrated with the deployment of the nearby temporary stations. Thus, the scattered distribution of early aftershocks may be caused by poor location accuracy. Along the seismic sequence from the NW to the SE, the focal depth become shallower, and the focal depth in the NW segment reaches to about 12 km and 10 km in the SE segment. The depth of early earthquakes is more uniform, and later earthquakes are relatively clustered at the NW and SE ends. Cross section perpendicular to the seismogenic fault shows that tilted fault plane dips to the SW with steep angle (Fig. 4b).

4. DISCUSSION

4.1 Fine-scale structure of the seismogenic fault

The focal mechanism solutions of the Yangbi mainshock released by USGS and GCMT are as follows (strike/dip/rake): $135^{\circ}/82^{\circ}/-165^{\circ}$ and $315^{\circ}/86^{\circ}/168^{\circ}$. The results are consistent and both indicate that this earthquake is a strike-slip earthquake (Fig. 1). Our seismic sequence revealed that the strike of the fault plane is about 140° , with a steep dip-angle dipping to the SW. The crustal anisotropy study shows (Wu et al., 2020) that different fast polarization directions on its east and west sides of the Weixi-Qiaohou-Weishan fault, and the principal compressive stress direction on the west side is NNW. In addition, studies on the focal mechanisms (Xu et al., 2020) and the Global Positioning System (GPS) measurements (Wang and Shen, 2020) also revealed that the direction of regional stress field in this study area is NNW, which is favorable to the southeastward rupture.

We plotted seven seismic cross-section profiles along the aftershock zone and analyzed the geometric features of the seismogenic fault (Fig. 5). Profiles AA'-GG' show earthquake distribution from the north to the south (Fig. 5c~i). The distance from each earthquake to the

profile is less than 0.5 km, except the profile AA', which is less than 1.0 km. Overall, the earthquakes perpendicular to the line LL' are nearly vertical and consistent with the high-angle fault pattern around the region of the Weixi-Qiaohou-Weishan fault. Profiles AA' and CC' (Fig. 5c~e), located at the northwestern end of the seismic sequence, indicate that the main fault dips to the SW, with a dip-angle of about 80°. While seismic distribution of profiles DD'-FF' is aggregated, and the linear alignment is not obvious (Fig. 5f~h). Profile GG' crossing the main fault at the southeast end reveal three parallel high dip-angle faults also dipping to the SW (Fig. 5i). Accordingly, we speculate that the seismogenic fault of the Yangbi earthquake is a high dip-angle fault, which has a simple structure in the north and more complicate structure in the south consisting of at least three branching faults. While in the middle zone, the earthquake distribution is slightly scattered due to the transformation of the fault structure. From the focal mechanism results of small and medium earthquakes, ruptures in the northern section shows predominantly a strike-slip type but in the southern section with varying types of normal/strike-slip/thrust (Fig. 5b, Yang et al., 2021), further supporting our observation of the morphology changes of the fault structure. In addition, a small cluster of earthquakes occurred in the north of the main rupture zone shows that the dip-angle of the fault there is steep, and the strike of this fault is likely in the NNE direction from the alignment of the aftershocks (Fig. 5a).

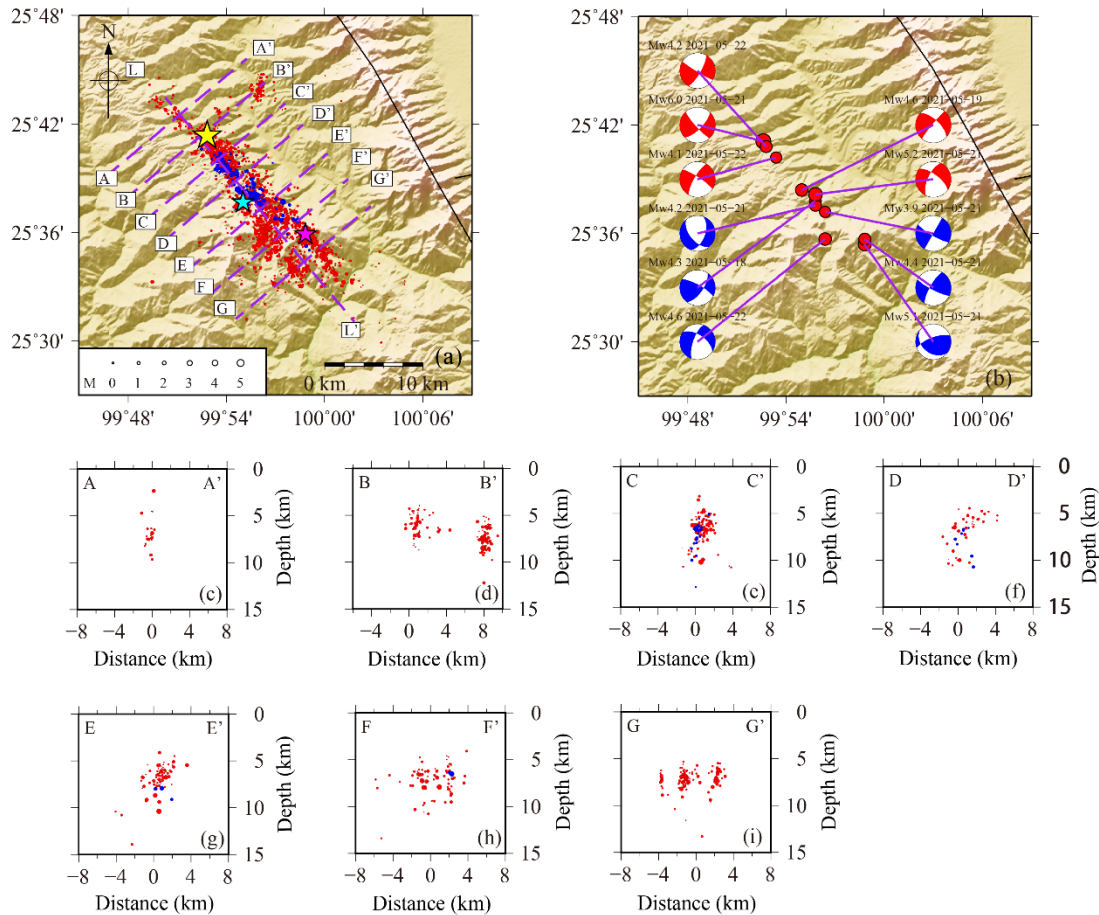


Figure 5. Focal depth cross-sections across the main fault. (a) Location of the profiles. The yellow, cyan and magenta stars denote the mainshock, the largest foreshock and the largest aftershock, respectively. (b) Focal mechanism of the earthquakes of $M \geq 4.0$ (Yang et al., 2021). The red and blue beach balls represent focal mechanism results in the northern and southern section of the faults, respectively. (c~i) Earthquake distribution along each profile. The distance from each earthquake to the profile AA' is less than 1.0 km, and that to other profiles is less than 0.5 km. Blue and red dots represent foreshocks and aftershocks.

Narrow Quaternary basins, including the Madeng basin and the Weishan basin, are developed in the northern and southern sections of the Weixi-Qiaohou-Weishan fault, while the basins in the middle section are fewer and smaller in size (Fig. 1, Institute of Geology, National Seismological Bureau, et al., 1990). An $M_s 5.5$ Eryuan earthquake occurred in the northern area of the middle section of this fault in 2013, and the seismogenic fault was the NNW-striking eastern margin fault of the Liantie Basin (Fig. 1). From results of the field geological survey and remote sensing image interpretation, this seismogenic fault consists of at least three parallel faults (Huang et al., 2015). Because the surface rupture corresponding to the area of this Yangbi earthquake has not revealed by the current geological survey data, we speculate that the Yangbi earthquake occurred in an unmapped secondary fault which lies on the southwest side of the Weixi-Qiaohou-Weishan fault,

which is similar to its northern region. Considering the Riedel shear structures and segmented faults are common in strike slip zones in the form of *en echelon* (Davis et al., 2000; Katz et al., 2004), we infer that the three faults in the SE segment revealed by the seismic sequence may be connected to the subsidiary fractures by the Riedel shearing.

4.2 Foreshock activity of the Yangbi earthquake

Ross et al. (2020) found that 72% of the mainshocks were preceded by foreshock activity through a study of the high-resolution earthquake catalog of $M \geq 4$ for Southern California from 2008-2017. Thus, foreshock activity prior to the occurrence of the mainshock may be observed in some moderate-to-strong mainshocks. In the case of the Yangbi earthquake, starting from May 18, 2021, abundant seismic activity preceded the mainshock is spatially manifested by clustering around the mainshock. Earthquakes before the mainshock was mainly distributed between the largest foreshock and the mainshock, and seismicity after $M_s5.6$ earthquake mainly expanded to the SE direction (Fig. 6a).

From the analysis of the time series (Fig. 6b), a 15-day period of earthquake quiescence existed before May 18. After that day, the frequency of earthquakes increased. However, the seismic frequency dramatically decreases on the day before the mainshock. Compared with the $M7.3$ Haicheng earthquake in 1975, which is a successful forecasting event, also had a similar obvious foreshock activity and a temporary quiescence before the mainshock occurred (Wang et al., 2006). The foreshocks of the Haicheng earthquake were tightly clustering (Jones et al., 1982) and the focal mechanisms of foreshocks were similar to that of the mainshock (Chen et al., 1999), which is also exhibited in this Yangbi earthquake.

As foreshocks are the most distinct precursory signals to the mainshock, probing the relationship between the foreshocks and mainshock is vital to understanding the earthquake nucleation process. Two end-member conceptual models are used to explain this process: pre-slip model (Dodge et al., 1996) and cascade model (Beroza and Ellsworth, 1996). A scaling relationship between the radius of the foreshocks zone and the seismic moment of the mainshock in California was brought up by Dodge et al. (1996), which is consistent with the pre-slip model. In the Yangbi earthquake, the radius of the foreshocks zone ($\sim 3\text{km}$) is much larger for the upcoming $M_s6.4$ mainshock, so it does not support the pre-slip model. Combined with fine-scale structure of the faults revealed in last chapter, as well as earthquakes before and after the $M_s5.6$

foreshock little overlap with each other (Fig. 6a), we infer that the rupture zone of the foreshock before and after the $M_s5.6$ foreshock belong to different segment of the faults. Earthquakes before the $M_s5.6$ foreshock (gray circles in Fig. 6a) have loaded the stress on its neighboring fault and triggered the $M_s5.6$ foreshock. The following $M_s6.4$ mainshock was triggered by the $M_s5.6$ foreshock with the stress accumulated to critical rupture, which is consistent with cascade model. From the current earthquake catalog, the migration of foreshock activity to the mainshock is not comprehensive. By analyzing a more complete catalog of earthquakes, e.g., artificial intelligence (AI) based phase-picking catalog, it is helpful to better understanding the earthquake nucleation process.

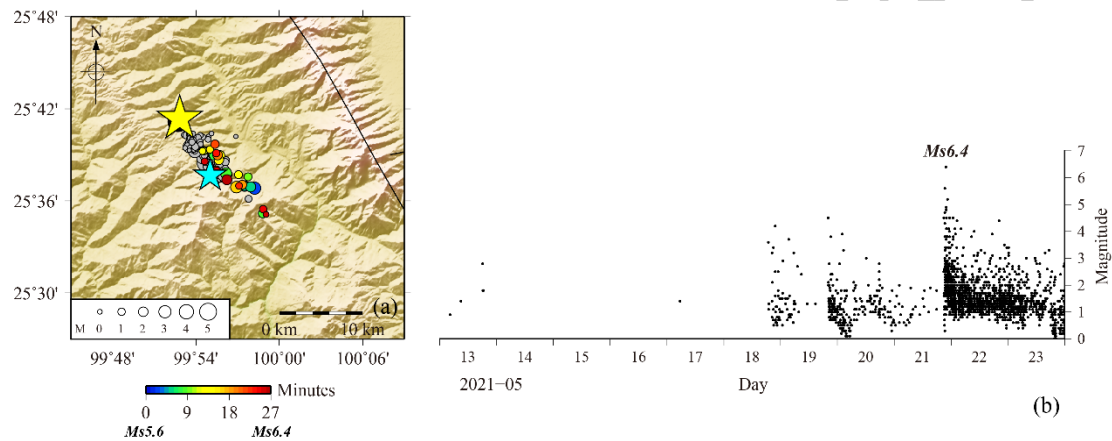


Figure 6. Foreshock activity of the Yangbi earthquake. (a) Seismic activity three days before the mainshock after relocation, gray circles indicate earthquakes before the largest foreshock $M_s5.6$, circles with colors indicate earthquakes between the time period of the largest foreshock and the mainshock. The yellow and cyan stars denote the mainshock and the largest foreshock, respectively. Colors of the earthquakes indicate the origin time relative to the largest foreshock. (b) M-T diagram of the Yangbi earthquake with different time-scale. The earthquake catalog data is from the observation bulletin.

4.3 Relationship between the velocity structure and the Yangbi earthquake

Velocity structure imaging in and around the area of the Yangbi earthquake shows a clear low-velocity layer in the middle crust (Hu et al. 2005; Xu et al. 2013; Yang et al. 2014; Bao et al., 2015; Chen et al. 2016; Liu et al., 2021; Gao et al., 2021). High conductivity properties beneath the study area were also revealed by magnetotelluric method studies (Sun et al., 1990; Bai et al., 2001). Zhang et al. (2020) used data from 43 dense seismic stations in this region by receiver function method, and found that the northern and middle sections of the Weixi-Qiaohou-Weishan fault area are Poisson's ratio high gradient zones. The observations of low seismic velocity anomalies, high conductivity, and high Poisson's ratio suggest that fluid may exist in the middle

crust of the study area. Wang et al. (2021) considered that fluid in the source region plays a critical role in the generation of earthquakes, since the presence of fluid would lead to the build-up of high pore pressure around the mainshock fault, and lower the threshold for fault close to failure.

Wang et al. (2002) found that most of the strong earthquakes in the Sichuan-Yunnan region occurred in the middle and upper crust with high velocity anomalies or normal velocity structures, and low velocity layers were prevalent beneath them. Previous researches revealed that many large earthquakes occurred at the boundary between high- and low-velocity anomalous zones, e.g., 2004 mid Niigata prefecture $M6.8$ earthquake (Korenaga et al., 2005), 2016 South Taiwan $Mw6.4$ earthquake (Toyokuni et al., 2016), 2016 Kumamoto $M7.3$ earthquake (Yano and Matsubara, 2017), 2011 Tohoku $Mw9.0$ earthquake (Hua et al., 2020). Wang and Kao (2019) revealed that more than 70% of large crust earthquakes ($M \geq 6.0$) during 1905-2018 occurred in Taiwan were located at the low-to-high velocity boundary. They suggest that large amount of fluids can be released from the low-velocity zone, and it is likely that the fluids will migrate into the high-velocity side where the materials are less porous with less saturation rate. The change of hydrological properties may lead to high pore pressure along the velocity boundary that, in turn, reduces the mechanical strength of rocks and facilitates seismogenesis. Figure 7 shows that the Yangbi earthquake occurred in the boundary between the high- and low-velocity zone. We presumed that the fluids released from the low-velocity zone migrating to the upper high-velocity seismogenic layer lead to high pore pressure in the source area and decrease the strength of the mainshock fault, which may be the causation of the Yangbi earthquake.

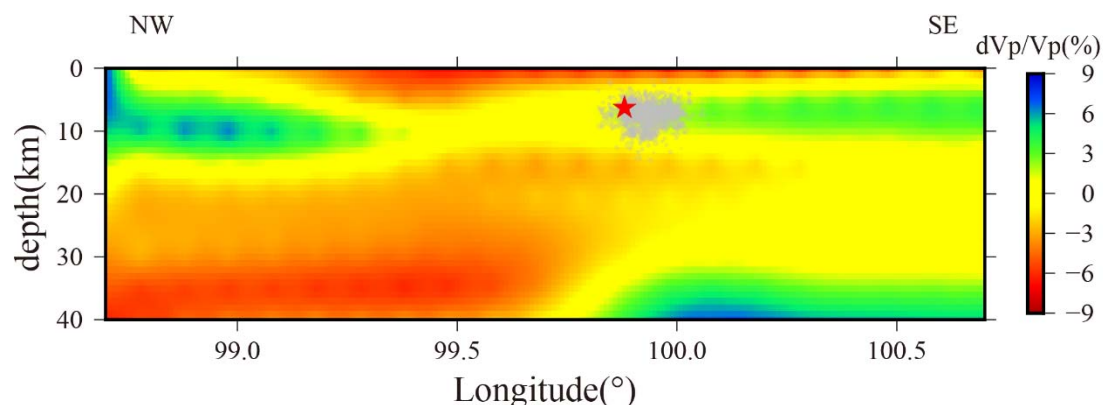


Figure 7. Crustal velocity structure in the source region of the Yangbi earthquake.

The negative and positive percentage of dVp/Vp represent low- and high-velocity, respectively. Cross-section of the seismic velocity along the strike of the main fault is referred to Liu et al. (2021). Red star indicates the mainshock, and the gray circles represent the foreshocks and aftershocks of the Yangbi earthquake.

Due to the weak historical seismicity of the Weixi-Qiaohou-Weishan fault compared to the adjacent northern segment of the Red River fault zone, studies in this region were scarce (Chang et al., 2016a). However, since the northwest Yunnan has been selected as a fault meta-instability experimental site in 2017, the Weixi-Qiaohou-Weishan fault has received increasing attention. Historical seismic data indicate that the northern and southern sections of the Weixi-Qiaohou-Weishan fault have experienced the Madeng and Weishan $6_{1/4}$ earthquakes, respectively, while no earthquakes of $M \geq 6$ have ever occurred in the middle section (Huang et al., 2015). Before the Yangbi $M_s6.4$ earthquake, the largest earthquake assessed in the middle section of the Weixi-Qiaohou-Weishan fault was of M 5-6. This $M_s6.4$ earthquake was the first earthquake of $M \geq 6$ in the middle section of this fault zone, and as a boundary fault connecting the Jinsha River fault and the Red River fault, the seismic activity hazard of the Weixi-Qiaohou-Weishan Fault needs to be further assessed.

5. CONCLUSIONS

In this paper, we relocated 2133 foreshocks and aftershocks of the Yangbi $M_s6.4$ earthquake sequence on the basis of the seismic observation bulletin from the Yunnan seismic network by using the double-difference location method. The main findings are as follows:

(1) Aftershocks were mainly distributed on the southwest side of the middle section of the Weixi-Qiaohou-Weishan fault zone, with a NW-trending alignment along the fault and dipping steeply to the SW. The strike of faults in the main rupture zone are about 140° , with the length of ~ 25 km. The focal depths of most earthquakes are shallower than 12 km.

(2) The distribution of aftershocks is narrow on the northwestern side and wide on the southeastern side, reflecting the complex fault structure of the Yangbi earthquake. A relatively simple steep-dipping strike-slip fault is shown in the northern section, while at least three branching faults exist in the southern section.

(3) This earthquake sequence has obvious foreshock activity and rich aftershocks. Earthquakes before and after the $M_s5.6$ foreshock little overlap with each other, indicates that they occurred on different segment of the faults. Earthquakes before the $M_s5.6$ foreshock have loaded the stress on its neighboring fault and triggered the $M_s5.6$ foreshock. The following $M_s6.4$ mainshock was triggered by the $M_s5.6$ foreshock, which is consistent with cascade model.

(4) The Yangbi $M_s6.4$ earthquake occurred in the boundary between the high- and low-velocity anomalous zones. Low seismic velocity anomalies, high conductivity, and high Poisson's ratio suggest the existence of the fluid in the study area, which may lead to high pore pressure in the source region and lower the strength of the mainshock fault, thus facilitates the generate of the Yangbi earthquake.

This earthquake is the largest earthquake that occurred on an unmapped secondary fault which lie on the southwest side of the middle section of the Weixi-Qiaohou-Weishan fault, thus earthquake hazard of the Weixi-Qiaohou-Weishan fault needs to be further evaluated by in conjunction with the fine-scale structure of the faults revealed by the relocated aftershocks.

ACKNOWLEDGEMENTS

We thank the China Earthquake Networks Center and the Yunnan Earthquake Agency for providing seismic phase data of the Yangbi earthquake. We also gratefully acknowledge Prof. Dun Wang, associate Prof. Wenkai Chen for the invitation of this special issue. We thank Prof. Zhonghai Wu, Dr. Xiaolong Huang and two reviewers for their comments and suggestions which has greatly improved this manuscript. The relocated aftershock sequence catalog determined in this study is uploaded in the web version of the attached file Yangbi_reloc.txt, which is also available from the China Earthquake Science Data Center (<http://www.chinarraydmc.cn/highlights/queryPage?mid=44&mpid=28>). All the figures were plotted using Generic Mapping Tools (Wessel and Smith, 1998). This work was financially supported by National Science Foundation of China (Grant No. 41774067), the National Key R&D Program of China (Grant No.2018YFC1503400) and the Special Fund of the Institute of Geophysics, China Earthquake Administration (Grant No. DQJB20X07).

REFERENCES CITED

- Bai, D., Unsworth, M.J., Meju, M.A., et al., 2010. Crustal deformation of the eastern Tibetan plateau revealed by magnetotelluric imaging. *Nature Geoscience*, 3(5):358-362.
- Bai, Z.M., Wang, C.Y., 2004. Tomography research of the Zhefang-Binchuan and Menglian-Malong wide-angle seismic profiles in Yunnan province. *Chinese Journal of Geophysics*, 47(2):257-267 (in Chinese with English Abstract).
- Bao, X.W., Sun, X.X., Xu, M.J., et al., 2015. Two crustal low-velocity channels beneath SE Tibet revealed by joint inversion of Rayleigh wave dispersion and receiver functions. *Earth and*

Planetary Science Letters, 415:16-24.

- Beroza, G.C., Ellsworth, W.L., 1996. Properties of the seismic nucleation phase. *Tectonophysics*, 261: 209– 227.
- Chang, Z.F., Chang, H., Li, J.L., et al., 2016a. The characteristic of active normal faulting of the southern segment of Weixi-Qiaohou fault. *Journal of Seismological Research*, 39(4):579-586 (in Chinese with English Abstract).
- Chang, Z. F., Chang, H., Zang, Y., et al., 2016b. Recent active features of Weixi-Qiaohou fault and its relationship with the Honghe fault. *Journal of Geomechanics*, 22(3):517-530 (in Chinese with English Abstract).
- Chen, J.H., Liu, Q.Y., Li, S.C., et al., 2009. Seismotectonic study by relocation of the Wenchuan M_s 8.0 earthquake sequence. *Chinese Journal of Geophysics*, 52:390-397 (in Chinese with English Abstract).
- Chen, S.W., Wang, B.S., Tian, X.F., 2016. Crustal structure from Yunxian-Ninglang wide-angle seismic reflection and refraction profile in Northwestern Yunnan, China. *Dizhen Dizhi*, 38(1):91-106 (in Chinese with English Abstract).
- Chen, Y., Liu, J., Ge, H., 1999. Pattern characteristics of foreshock sequences. *Pure and Applied Geophysics*, 155(2-4):395-408.
- Davis, G. H., Bump, A. P., Garca, P. E., Ahlgren, S. G., 2000. Conjugate riedel deformation band shear zones. *Journal of Structural Geology*, 22(2):169-190.
- Dodge, D.A., Beroza, G.C., Ellsworth, W.L., 1996. Detailed observations of California foreshock sequences: Implications for the earthquake initiation process. *Journal of Geophysical Research*, 101(B10), 22:371– 392.
- Fang, L.H., Wu, J.P., Wang, W.L., et al., 2015. Aftershock Observation and Analysis of the 2013 M_s 7.0 Lushan Earthquake. *Seismological Research Letters*, 86(4):1135-1142.
- Fang, L.H., Wu, J.P., Su, J.R., et al., 2018. Relocation of mainshock and aftershock sequence of the M_s 7.0 Sichuan Jiuzhaigou earthquake. *Chinese Science Bulletin*, 63:649-662 (in Chinese with English Abstract).
- Gao, T.Y., Ding, Z.F., Wang, X.C., et al., 2021. Joint inversion of receiver functions, Reyleigh wave dispersion and ZH ratio for crustal structure in Southeast Tibetan Plateau and its implications for dynamics. *Chinese Journal of Geophysics*, 64(6):1885-1906 (in Chinese with English Abstract).
- Hua, Y., Zhao, D., Toyokuni, G., & Xu, Y., 2020. Tomography of the source zone of the great 2011 Tohoku earthquake, *Nature Communications*, 11(1):1163.
- Huang, X.L., Wu, Z.H., Jiang, Y., et al., 2015. Seismic intensity distribution and seismogenic structure analysis of the March 3, 2013 Eryuan M_s 5.5 earthquake in Dali, Yunnan Province. *Geological Bulletin of China*, 34(1):135-145 (in Chinese with English Abstract).
- Institute of Geology, China Earthquake Administration, Yunnan Earthquake Agency, 1990. Active faults in the Northwest Yunnan Region. Seismological Press, Beijing.
- Jones, L.M., Wang, B., Xu, S., et al., 1982. The foreshock sequence of the February 4, 1975, Haicheng Earthquake ($M = 7.3$). *Journal of Geophysical Research*, 87(B6):4575-4584.
- Katz, Y., Weinberger, R., Aydin, A., 2004. Geometry and kinematic evolution of Riedel shear structures, Capitol Reef National Park, Utah. *Journal of Structural Geology*, 26(3):491-501.
- Korenaga, M., Matsumoto, S., Iio, Y., et al., 2005. Three dimensional velocity structure around aftershock area of the 2004 mid Niigata prefecture earthquake ($M_6.8$) by the

- Double-Difference tomography. *Earth, Planets and Space*, 57(5):429-433.
- Lanza, F., Chamberlain C.J., Jacobs K., et al., 2019. Crustal Fault Connectivity of the Mw 7.8 2016 Kaikōura Earthquake Constrained by Aftershock Relocations. *Geophysical Research Letters*, 46(12):6487-6496.
- Laske, G., Masters, G., Ma, Z., et al., 2013. Update on CRUST1. 0—A 1-degree global model of Earth's crust. EGU General Assembly Vienna, Austria. 2658.
- Li, Y., Wang, D., Xu, S., et al., 2019. Thrust and conjugate strike-slip faults in the 17 June 2018 M_{JMA} 6.1 (Mw 5.5) Osaka, Japan, earthquake sequence. *Seismological Research Letters*, 90(6):2132-2141.
- Liu, Y., Yao, H.J., Zhang, H.J., et al., 2021. The Community Velocity Model V1.0 of southwest China, constructed from joint body - and surface - wave traveltime tomography. *Seismological Research Letters*. <https://doi.org/10.1785/0220200318>.
- Momeni, S. M., Tatar, M., 2018. Mainshocks/aftershocks study of the August 2012 earthquake doublet on Ahar-Varzaghan complex fault system (NW Iran). *Physics of the Earth and Planetary Interiors*, 283:67-81.
- Ren, J. J., Zhang, S. M., Hou, Z. H., et al. 2007. Study of late quaternary slip rate in the mid-segment of the Tongdian-Weishan fault. *Seismology and Geology*, 29(4):756-764 (in Chinese with English Abstract).
- Ross, Z.E., Cochran E.S., Trugman, D.T., 2020. 3D fault architecture controls the dynamism of earthquake swarms. *Science*, 368:1357-1361.
- Sun, J., Xu, C.F, Jiang, Z, et al., 1989. The electrical structure of the crust and upper mantle in the west part of Yunnan province and its relation to crustal tectonics. *Seismology and Geology*, 11(1):35-45 (in Chinese with English Abstract).
- Tang, P., Chang, Z.F., 2013. Study on the activity of the Weishan Basin section of the Wixi-Qiaoghou Fault. *Geological review*, 59:108-109 (in Chinese).
- The Earthquake Disaster Prevention Department of China Earthquake Administration, 1999a. Catalogue of Chinese Historical Strong Earthquakes. China Science and Technology Press, Beijing.
- The Earthquake Disaster Prevention Department of China Earthquake Administration, 1999b. Catalogue of Chinese Present Earthquakes. China Science and Technology Press, Beijing.
- Toyokuni, G., Zhao, D., & Chen, K.H., 2016. Tomography of the source zone of the 2016 South Taiwan earthquake. *Geophysical Journal International*, 207:635-643.
- Waldhauser, F., Ellsworth, W.L., 2000. A double-difference earthquake location algorithm: Method and application to the northern Hayward fault, California. *Bulletin of the Seismological Society of America*, 90:1353-1368.
- Wang, C.Y., Mooney W.D., Wang, X.L., et al., 2002. Study on 3-D velocity structure of crust and upper mantle in Sichuan-Yunnan region, China. *Acta Seismologica Sinica*, 24(1):1-16 (in Chinese with English Abstract).
- Wang, K., Chen, Q.F., Sun, S., et al., 2006. Predicting the 1975 Haicheng earthquake. *Bulletin of the Seismological Society of America*, 96(3):757-795.
- Wang, M., Shen, Z.K., 2020. Present-Day Crustal deformation of continental China derived from GPS and its tectonic implications. *Journal of Geophysical Research: Solid Earth*, 125(2): e2019JB018774.
- Wang, Z., Kao, H., 2019. The Significance of Tomographic Edge Zones for Large Earthquakes in

- Taiwan. *Journal of Geophysical Research: Solid Earth*, 124(11), 11822-11839.
- Wang, Z., Wang, J., Yang, X., 2021. The Role of Fluids in the 2008 Ms8.0 Wenchuan Earthquake, China, *Journal of Geophysical Research: Solid Earth*, 126(2), e2020JB019959.
- Wessel, P., Smith, W., 1998. New, improved version of the Generic Mapping Tool released, *Eos Transactions American Geophysical Union*, 79(47), 579.
- Wu, P., Gao, Y., Chen, A.G., et al., 2020. Preliminary study on the anisotropy of the upper crust in the Sanjiang area, southeastern margin of the Tibetan Plateau. *Chinese Journal of Geophysics*, 63(3):1104-1116 (in Chinese with English Abstract).
- Xie, Z., Zheng, Y., Yao, H. et al., 2018. Preliminary analysis on the source properties and seismogenic structure of the 2017 Ms7.0 Jiuzhaigou earthquake. *Science China Earth Science*, 61:339–352 (in Chinese with English Abstract).
- Xu, Y., Koper, K.D., Burlacu, R., et al., 2020. A new uniform moment tensor catalog for Yunnan, China, from January 2000 through December 2014. *Seismological Research Letters*, 91(2A): 891-900.
- Xu, Y., Yang, X.T., Liu, J.H., 2013. Tomographic study of crustal velocity structures in the Yunnan region southwest China. *Chinese Journal of Geophysics*, 56(6):1904-1914 (in Chinese with English Abstract).
- Yang, T., Wu, J.P., Fang, L.H., et al., 2014. 3-D crustal P-wave velocity structure in western Yunnan area and its tectonic implications. *Dizhen Dizhi*, 36(2):392-404 (in Chinese with English Abstract).
- Yang, Z.G., Liu, J., Zhang X.M., et al., 2021. A preliminary report of the Yangbi, Yunnan, MS6.4 earthquake of May 21, 2021. *Earth and Planetary Physics*, 5(4):1–3.
- Yang Q.Y., Wu Q.J., Sheng, Y.R., et al., 2018. Regional seismic body wave tomography and deep seismogenic environment beneath Zhangbo seismic belt and its adjacent area. *Chinese Journal of Geophysics*, 61(8):3251-3262 (in Chinese with English Abstract).
- Yano, T.E., Matsubara, M., 2017. Effect of newly refined hypocenter locations on the seismic activity recorded during the 2016 Kumamoto Earthquake sequence. *Earth, Planets and Space*, 69(1):74.
- Yi, G.X., Long, F., Liang, M.J., et al., 2019. Focal mechanism solutions and seismogenic structure of the 17 June 2019 M_s 6.0 Sichuan Changning earthquake sequence. *Chinese Journal of Geophysics*, 62:3432-3447 (in Chinese with English Abstract).
- Yu, X.W., Chen, Y., Zhang, H., 2010. Relocation of Earthquakes in Beijing-Tianjin-Tangshan Region with double-difference Tomography Technique. *Acta Seismologica Sinica*, 32(3):257-269 (in Chinese with English Abstract).
- Zhang, G.W., Lei, J.S., Liang, S.S., et al., 2014. Relocations and focal mechanism solutions of the 3 August 2014 Ludian, Yunnan M_s 6.5 earthquake sequence. *Chinese Journal of Geophysics*, 57:3018-3027 (in Chinese with English Abstract).
- Zhang, T.J., Jin, M.P., Liu, Z.F., et al., 2020. Distribution and significance of crustal thickness and Poisson's ratio in Northwestern Yunnan. *Journal of seismological research*, 43(1):10-18 (in Chinese with English Abstract).
- Zhang, Z., Gao, Y., 2019. Crustal thicknesses and Poisson's ratios beneath the Chuxiong-Simao Basin in the Southeast Margin of the Tibetan Plateau, *Earth and Planetary Physics*, 3(1):69-84.
- Zhao, B., Gao, Y., Huang, Z.B., et al., 2013. Double difference relocation, focal mechanism and

stress inversion of Lushan $M_S7.0$ earthquake sequence. *Chinese Journal of Geophysics*,
56:3385-3395 (in Chinese with English Abstract).

JES Unedited